

Road detection in dense urban areas using SAR imagery and the usefulness of multiple views

Florence Tupin, Bijan Houshmand, Mihai Datcu

Abstract—This paper deals with the automatic extraction of the road network in dense urban areas using a few meter resolution SAR images. The first part presents the proposed method which is an adaptation of previous work to the specific case of urban areas. The major modifications are: first, the clique potentials of the Markov Random Field which extracts the road network are adapted; secondly, a multi-scale framework is used. Results on shuttle mission and aerial SAR images with different resolutions are presented. The second part is dedicated to road extraction combining 2 SAR images taken with different flight directions (orthogonal and anti-parallel passes) and the obtained improvement is analyzed.

Index Terms—road detection, SAR images, Markov Random Fields, different orientation views

I. INTRODUCTION

SATELLITE remote sensing has reached a new level of sophistication. There are at present many synthetic aperture radar (SAR) sensors providing a wide area coverage of the earth (either satellite sensors like ERS-2, Radarsat and soon EnviSat, and shuttle missions [1] [2], or even aerial acquisitions [3]) due to their all-time capabilities. Small-scale, higher resolution imagery is required for detailed work. In this respect the new generations of a few meter resolution SAR sensors will open the way to novel applications. However, the available interpretation methodologies cannot cope with the high complexity and huge amounts of acquired data. Many valuable data sets are unexplored.

The article presents and demonstrates solutions for one of the most relevant applications of a few meter resolution SAR data: road network detection in dense urban areas. Although many algorithms have already been proposed for optical remote-sensing images [4], their application to SAR data remains difficult due to speckle noise. Indeed their direct application provides poor results, and their performance depends on the radiometric mean of a region in the SAR image. Therefore, dedicated works have been developed to deal with radar images and their specific properties [5].

Nevertheless, only very few works deal with road extraction in dense urban areas [6]. The particular properties of these areas can disturb the detection process in two ways: first, the backscattering mechanisms are specific to these areas implying different statistical laws; secondly, the network characteristics

are also specific (higher frequency of cross-roads, multiple networks with different widths,...). The subject of this paper is the introduction of a road detection algorithm for urban environment. We present an adaptation of a previous method [7]. This method has proven to be efficient on radar images but is not well adapted to urban areas. Indeed, the prior knowledge introduced in [7] is not valid in this case.

The first part of this article presents the proposed method which is a modification of a road detection algorithm for non-urban areas [7]. The new clique potentials are introduced and the multi-scale process is described. Results of the method are then presented for two American cities: New-York and San-Francisco. In the second part, we study the potential improvement when images taken from 2 different flight directions are available. First, the merging method is described and then the results in the case of orthogonal (New-York area) and anti-parallel (San-Francisco area) directions are presented.

II. ROAD DETECTION IN DENSE URBAN AREAS

A. Appearance of the road network in urban areas

The road network usually appears as dark lines in SAR data. This is due to the smoothness of the road compared to its surrounding structures, thus having a mirror like reflection resulting in low radar signal returns. The effect is more pronounced for roads oriented in range direction. In azimuth direction, some specific configurations like border lines of highways, road rails, elevated roads, bridges, etc., make roads to appear as very bright lines because of multiple bounce scatterings.

In the case of urban areas, roads also appear as dark lines, and the contrast with its surroundings is usually higher than in non-urban areas due to the double bounce reflections of the buildings. Nevertheless, the following phenomena must be kept in mind:

- the heights of the building induce some lay-over effects, and thus the accurate position of the roads is hard to define; depending on the street orientation and the incidence angle, there may be some discrepancy between the detected roads and their real position;
- if the buildings are too high compared to the incidence angle and the street too narrow, the roads may not be visible on the radar image; in this case, some parts of the streets may not be available on the radar data.

The difference in appearance depending on range or azimuth directions makes the merging of different views very useful as presented in section III.

F. Tupin is with the Signal and Image Processing Department of Télécom Paris, 75634 Paris Cedex, France, (email: florence.tupin@enst.fr)

B. Houshmand is with the Jet Propulsion Laboratory, 4800 Oak Grove Drive, Pasadena, CA.

M. Datcu is with the DLR-IMF, Oberpfaffenhofen, D-82234 Wessling, Germany.

B. Description of the method

The road detection method proposed in [7] is divided into two main steps, which are summed up here (see also the diagram of fig.1):

- as a first step of feature extraction (section II.B.1), a line detector adapted to the speckle statistics of SAR images is applied (thresholding and linking provide segments that are candidates for belonging to the network);
- secondly, the “network reconstruction” step (section II.B.2), a closure method based on a Markovian approach defined on a graph of segments is performed; this step is a labeling of the segment graph with labels “road” and “not-road” by minimizing an energy function; this function, derived from probabilities and from a Markovian hypothesis made on the label field, takes both original data and prior knowledge about the road shape (probability of crossings and curvature limitations) into account.

In the following sections we detail these different phases of the process, emphasizing the adaptation of the algorithm to the urban areas.

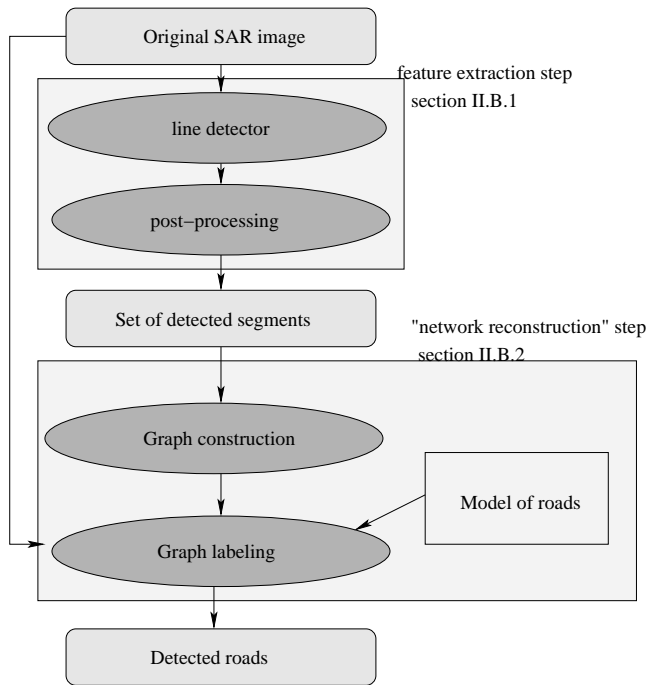


Fig. 1. Diagram of the proposed method for road detection

1) Feature extraction: In this step, the segments which are candidates for belonging to the road network are extracted using a line detector applied on the SAR image (first block of fig.1). This line detector is based on the statistical properties of fully developed speckle areas [8] and corresponds to the fusion of a ratio-based [9] and a correlation-based detector. In the case of Gamma distributed amplitude image (fully developed speckle [10]), a statistical study of the line detector gives the false alarm and detection rates depending on certain parameters (contrasts on both sides of the linear structure, size of the moving window, etc.) [7]. Therefore, the threshold of the line responses may be deduced as a compromise between a chosen false-alarm rate and a minimum detectable contrast.

In the case of urban areas, the previous study is not valid. Indeed, the backscattering mechanisms in the case of buildings -or most of the urban man-made objects-, which are smooth compared to the wavelength, do not correspond to the fully developed speckle model [11] [12]. A simplified model corresponding to a strong reflector (specular backscattering in a particular orientation) surrounded by a rough region implies a Rice statistic, but in a more common case of a mixing of strong and weak reflectors inside a resolution cell, no statistical model is available. Besides, having to take into account more complicated distributions, large analysis windows are necessary, which is not compatible with the fine lines we want to detect. Moreover, in practice, the line detector used in [7] provides acceptable results for urban areas. Indeed, the contrast on both sides of the road is high due to the building responses.

Starting from the response of the line detector for each pixel, we now generate segment primitives for further processing by the following procedures: thresholding of the response image and thinning of the binary image [13]; then a polygonal approximation step gives a vectorial representation of the segments¹.

2) Network reconstruction step: We now deal with the segments previously detected, trying to suppress false alarms and to connect the “good” ones to obtain a fully connected network of the streets (second block of fig.1). The same scheme as in [7] is adopted (please refer to it for a detailed description of the following steps). Starting from the remark that local knowledge is generally sufficient to identify roads, Markovian modeling has been developed to deal with road identification.

Graph construction

A graph is built from the detected segments and all the connections between them². Let us denote by N the number of segments. Each segment is indexed by i and represents a node of the graph G . Two nodes are linked when their corresponding segments share an extremity (see fig.2). G is thus the “line-graph” of the graph of segments [15].

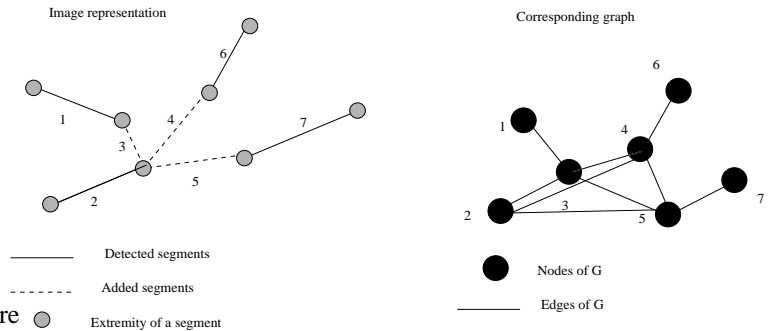


Fig. 2. Set of segments (detected and connections) and the corresponding graph

The cliques of the graph G are the complete sub-graphs of G which corresponds to all subsets of segments sharing an extremity, including singletons and cycles of three segments. Attributes are attached to the nodes and the arcs of G , taking into

¹Some of the local “cleaning” treatments proposed in [7] are no longer valid since they do not take into account the possibility of cross-roads; this is the case for the local Hough transform [14], which retains only the most predominant road in a window, thus suppressing the possible other parts of the cross-road.

²Actually, some proximity and alignment constraints are used to reduce the size of the graph.

account geometric properties:

- the attribute $\min(1, \frac{Length_i}{\mathcal{D}_{max}})$ is associated to each graph node i , where $Length_i$ is the segment length; \mathcal{D}_{max} will serve in the following as a scale factor which may be adjusted independently on the scene; this attribute is denoted by \mathcal{L}_i and takes its value in $[0, 1]$.
- the angle \mathcal{R}_{ij} modulo π between the 2 segments is associated to each arc between nodes i and j .

l_i is the label ($l_i \in \{0, 1\}$) associated to the node i , and l is the label configuration for the whole graph (collection of all the node labels).

Then the road identification process is modeled as the search of the “optimal” binary labeling l of the nodes of the graph (label 1 for road segments, 0 for others). The optimal labeling corresponds to the configuration l which minimizes an energy function derived from a probabilistic model (cf. [7]). This energy can be written as (with d the set of all the segment measures derived from the data):

$$U(l) = U_{\text{likelihood}}(l, d) + U_{\text{prior}}(l) \quad (1)$$

The first term $U_{\text{likelihood}}(l, d)$ measures the likelihood of the segments to belong to a road given the radiometric values of the SAR image and depending on the data. The second one $U_{\text{prior}}(l)$ reflects the a priori fit of the local configurations of the segments to a road hypothesis (contextual knowledge). Both terms are detailed in the following sections.

Likelihood term $U_{\text{likelihood}}(l, d)$

The observation d_i associated to each segment i is defined as the mean of the edge detector responses in the direction of the segment. The higher d_i is the more confidence we have that it could be a road.

The potential $V(d_i, l_i)$ associated to an observation d_i and a label l_i must be low for a “good” association (for instance low measure d_i and label 0 –“not-road”–). The potentials have been derived from a probabilistic study after a manual segmentation of roads by a human observer and is given by (see [7] for a detailed explanation):

$$V(d_i, l_i = 0) = 0 \text{ if } d_i < t_1 \quad (2)$$

$$V(d_i, l_i = 0) = \frac{d_i - t_1}{t_2 - t_1} \text{ if } t_1 < d_i < t_2 \quad (3)$$

$$V(d_i, l_i = 0) = 1 \text{ if } d_i > t_2 \quad (4)$$

$$V(d_i, l_i = 1) = 0 \quad \forall d_i \quad (5)$$

To respect the normalization constraint [7], the constant $\log Z$ is added to the potentials $V(d_i, l_i = 0)$, with $Z = t_1 + (1 - t_2)\frac{1}{e} - (t_2 - t_1)(\frac{1}{e} - 1)$ and $e = \exp(1)$. Since $Z < 1$, we have $\log Z < 0$. Besides, to take into account the length \mathcal{L}_i of the segments, the potentials are multiplied by \mathcal{L}_i .

The likelihood term is then defined by the sum of all the node potentials:

$$U_{\text{likelihood}}(l, d) = \sum_{i=1}^N V(d_i, l_i) \quad (6)$$

This term is not modified compared to the previous version of [7]. The main modifications are introduced in the contextual term which takes into account the prior information we have about the road shape.

Prior term $U_{\text{prior}}(l)$

In the Markovian framework, the prior (contextual) term can be written as a sum of the local clique potentials :

$$U_{\text{prior}}(l) = \sum_{c \in C} V_c(l_i, i \in c) \quad (7)$$

where C is the set of cliques ($V_c(l_i, i \in c)$ is simplified as $V_c(l)$ in the following).

Clique potentials have been chosen to express the following prior knowledge about roads in [7]:

- (i) roads are long (they should almost never stop),
- (ii) roads have a low curvature,
- (iii) intersections are rare (by this we mean that a segment is more often connected to a unique other segment in one of its extremities than to many segments, at least in non urban areas).

In the case of urban areas, the third point (iii) is no longer valid, and is replaced by the following assumptions:

- (iii) cross-roads with either “cross” or “T” shapes are frequent; cross-roads with more than 4 segments are rare.

The flexibility of the Gibbs field framework allows us to construct simple potentials endowing the random field with a probability distribution stemming from this prior knowledge. These potentials have been empirically chosen to express the previous constraints and are an extension of the previous work. Some simple parametric potentials have been defined with intuitive signification, as explained below. Supervised learning with neural networks as in [16] could also be done but some preliminary experiments showed that the size of the learning set has to be huge. Of course, the chosen model with “cross” or “T” cross-roads is restrictive and adapted to certain type of cities.

All clique potentials $V_c(l)$ are null except for the cliques of highest order corresponding to the sets of segments sharing the same common extremity for all segments, which turns out to be sufficient for modeling all the interactions between road segments given above. Denoting by \mathcal{A} an alignment criterion and \mathcal{P} a perpendicularity criterion, for a clique c of highest order, we define:

- $\forall i \in c, l_i = 0 \Rightarrow V_c(l) = 0$
- $\exists! i \in c / l_i = 1 \Rightarrow V_c(l) = K_e - K_{\mathcal{L}} \mathcal{L}_i$
- $\exists! (i, j) \in c^2 / l_i = l_j = 1, \mathcal{R}_{ij} > \frac{\pi}{2} \Rightarrow V_c(l) = -K_{\mathcal{L}} (\mathcal{L}_i + \mathcal{L}_j) + K_c \sin \mathcal{R}_{ij}$
- $\exists! (i, j, k, l) \in c^4 / l_i = \dots = l_l = 1, i\mathcal{A}j, k\mathcal{A}l, i\mathcal{P}k, j\mathcal{P}l \Rightarrow V_c(l) = -K_{\mathcal{L}} (\mathcal{L}_i + \mathcal{L}_j + \mathcal{L}_k + \mathcal{L}_l) + K_c (\sin \mathcal{R}_{ij} + \sin \mathcal{R}_{kl})$
- $\exists! (i, j, k) \in c^3 / l_i = l_j = l_k = 1, i\mathcal{A}j, i\mathcal{P}k, j\mathcal{P}k \Rightarrow V_c(l) = -K_{\mathcal{L}} (\mathcal{L}_i + \mathcal{L}_j + \mathcal{L}_k) + K_c (\sin \mathcal{R}_{ij} + \frac{1}{2}(\cos \mathcal{R}_{ik} + \cos \mathcal{R}_{jk}))$
- in all other cases $V_c(l) = K_i \sum_{i/i \in c} l_i$

All parameters are connected in a simple way with the three previously expressed road characteristics. Choosing $K_e > 0$

and $K_L > 0$ fulfills condition (i), and favors long roads (extremity penalty and length reward). $K_c > 0$ penalizes road configurations with high curvatures excepting cross-roads fulfilling conditions (ii) and (iii), whereas $K_i > 0$ puts crossroads with more than 3 or 4 parts and no “cross” or “T” shapes at a disadvantage, which corresponds to condition (iii). In practice the same study as in [7] can be used to define parameter intervals, but some typical values are: $K_e = 0.21$, $K_L = 0.12$ and $K_c = K_i = 0.3^3$. The figure 3 presents results showing the influence of the parameter values.

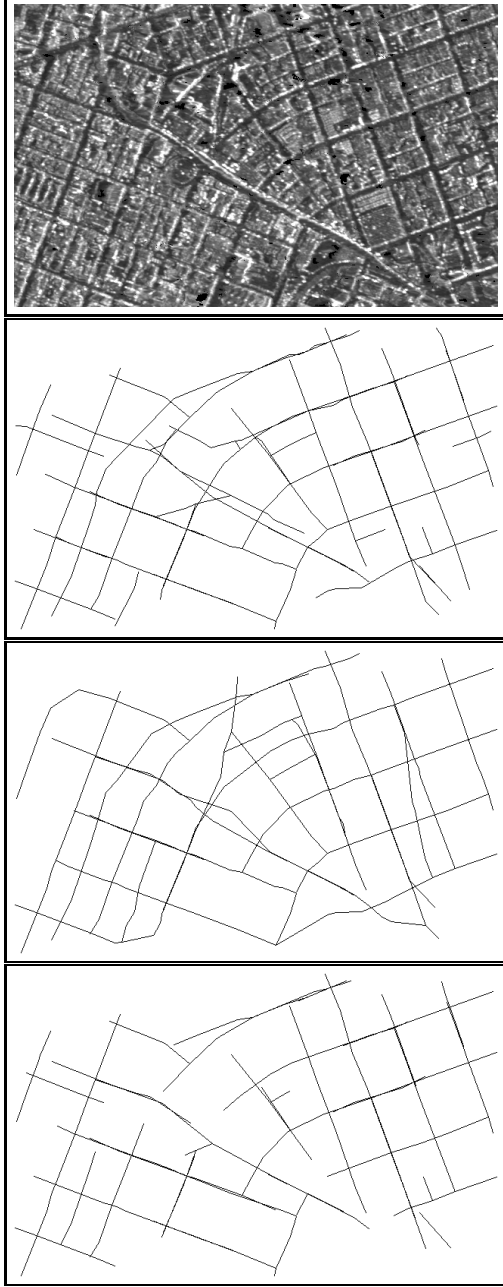


Fig. 3. Influence of the parameters illustrated on a small part (middle bottom) of the San Francisco image: top, default parameter set $K_e = 0.21$, $K_L = 0.12$ and $K_c = K_i = 0.3$; middle, with increased “extremity penalty” $K_e = 0.4$ (all other parameters are kept); bottom, with increased “angular penalty” $K_c = 0.8$ (and $K_e = 0.21$, $K_L = 0.12$).

³The parameter values are in fact identical to the ones of the previous work.

3) *Multi-scale analysis*: The road width is very variable on a remote sensing image, depending on the effective road size and the image resolution. The line detector of the line extraction step is limited to a line width of 5 pixels. To extract larger roads, a multi-scale process is applied. The number of scales to be considered is deduced from the pixel-spacing of the data.

Instead of detecting all the segment candidates and building a large graph for the connection step (and thus mixing all the networks), we prefer extracting the roads with different scales and then merging the networks with different widths. This method has the advantage of preserving the coherence of each network and produces less noisy results.

The multi-scale analysis is therefore made in the following way:

- creation of an image pyramid; the resolution is degraded by averaging the amplitudes of $n \times n$ pixel blocks; only two levels with $n = 2$ and $n = 4$ are considered here;
- extraction of the road network for each level by the previously described method (coarser when $n = 4$, and finer with the original image corresponding to $n = 1$);
- merging of the different networks by superimposition followed by a cleaning step.

C. Results

In this section we present the results on two large American cities, San Francisco and New York acquired by different sensors of a few meter resolution. The next satellite sensor generation should provide data with similar resolutions to the examples given below (6.25m for X-SAR and 2.5m for ERIM X-band IFSAR data).

1) *Results for X-SAR image (New York)*: This first example is an X-SAR image of New York (figure 4), acquired in October 94 during a SRL (Shuttle Radar Laboratory) mission. The pixel spacing is 6.25m×6.25m for a nominal resolution of 15.9m in range and 10m in azimuth. The incidence angle is 62.7° in ascending mode. The image is in ground-range geometry. It corresponds to the Brooklyn quarter with the Greenwood Cemetery and the Prospect Park in the upper left corner of the image (see the map figure 6d).

Automatic extraction provides the result presented in figure 6. The following comments can be made on the result: the main roads are detected; the network is incomplete (it misses some parts of the road); some false alarms occur in water areas due to the multi-scale process.

2) *Results for ERIM IFSAR image (San Francisco)*: This second example deals with an X-band, 80-MHz radar image of San-Francisco (figure 8) with a finer resolution, taken with ERIM sensor. This image is acquired by an aerial interferometric SAR system. The nominal radar incident angle at the center of the image is 45 degrees. The nominal resolution is 5 meters and pixel-spacing is 2.5 meters. The image is orthorectified as part of the interferometric processing. In addition to the radar image, the digital elevation model is also acquired.

Results are shown in fig.8 (bottom). Since the resolution is better, the road detection is improved compared to the previous result. Nevertheless, the same comments can be made: the whole organization of the network (density and direction) is



Fig. 4. X-SAR image of New York (Brooklyn) ©IMF-DLR (size is 2048×2048 pixels)

well detected (specially the low density of roads in the Golden Gate Park in the left of the image compared for instance to the upper right part); the false alarms in San Francisco Bay occur due to the presence of the bridge and some inhomogeneities in the water producing lines in the feature detection step. Note also, that although it is not very frequent, some connections in vegetation areas can occur due to the network reconstruction step of the method (this case occurs for instance in Alamo Square in the middle of the image).

III. USE OF MULTIPLE VIEWS WITH DIFFERENT ORIENTATIONS

Since radars are side looking sensors the direction of looking has a great influence on the acquired image [5]. This phenomenon is specially important for relief areas but also in dense urban areas, influencing road and building aspects. It is illustrated in figure 5 where the same area is seen with almost two orthogonal directions. In the first image (fig.5a), the sensor is on the left, and therefore horizontal roads (in the range direction) are easily visible. The buildings, which are perpendicular to the direction of looking (in azimuth direction) appear very bright due to double bounce reflections in “favorable” orientation, and the selected area has a very high radiometry compared to the whole SAR image. In the second image (fig.5b), the sensor is “above” the image, and therefore vertical roads are the most visible, whereas horizontal ones are more difficult to detect. The buildings do not have the same appearance as in fig.5a, and have a globally lower radiometry.

Not only the orientation has a great influence on the human-made structure aspect, but also the incidence angle value [11]; this is the case for instance for streets where high buildings

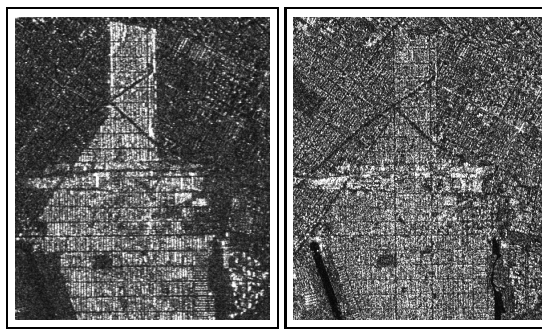


Fig. 5. Two SAR data with different looking directions: left image, the radar is on the left (looking right); right image, the radar is above (looking top to bottom)

stand along both sides of the road; in this situation, depending on the incidence angle, on the width of the streets and the height of the buildings, the roads may or not be visible on the radar image.

This part studies the road extraction improvement using different views of the same area. The first studied case is a very favorable one since the 2 views are almost perpendicular giving “orthogonal” information and the second one is the “worst case” with two anti-parallel directions.

The merging method has been described in [17] where two approaches were described: the first one was a simple superimposition of the two extracted networks and the second one a merging of the two SAR data inside the extraction process. Since the improvement using the second (more sophisticated) method was slight we only present here the results of the superimposition of the two detected networks. In all cases, the images are manually registered⁴.

A. Case of orthogonal views

We had at our disposal an almost perpendicular image of New-York, taken in descending mode, with an incidence angle of 31.6° . The result using the two perpendicular SAR images is shown in fig.6b and 6c. Comparing the result of figure 6b with the figure 6a, as expected we observe a clear improvement of the detected networks:

- some of the vertical streets which were not detected in a single view are now extracted (see for instance the bottom right of the image);
- some of the discontinuous roads are now complete which gives a better organization of the urban landscape (see for instance the top left of the image);
- some of the missed roads have been detected, so there are less undetected network parts (see for instance the darker area in-between the two very bright quarters).

In this case, the road network extraction is greatly improved using the 2 views with different orientations.

A quantitative analysis of the results showed that approximately only one third of the roads are detected on one image (in this particular area). Thus the percentage of detected roads is increased by around 30% compared to a single view.

⁴ Automatic registering using the two detected networks is the scope of some future work. Let us note here, that some registering problems may appear in dense urban areas due to the lay-over effects which are particularly important for the buildings.

B. Case of anti-parallel views

The processed images are JPL C-band AIRSAR images of San-Francisco (fig.7a), with a 40 MHz sensor and a nominal resolution of 10 meters in ground range and azimuth, and a pixel-spacing of 5 meters. The image is ortho-rectified using the interferometric process.

Here the problem is different, since the information is mainly redundant instead of complementary as in the previous case. Indeed, since the flights are parallel, the same road directions are favored. Therefore, in this case, the fusion of the two views is mostly useful to suppress some false alarms in the road detection process. The roads detected on both images are quite reliable whereas those appearing in only one view are suspected to be an erroneous detection.

The results are shown in fig.7b and c (due to the lack of space, only a small part is presented). The roads detected on both images are shown fig.7d. It only contains the main roads of the San-Francisco image. Some of the spurious streets found in between the real ones are suppressed. An analysis of the corresponding optical image has shown that the false detections are due to the specific organization of the town. Indeed, inside the square delimited by four roads, there are two rows of high buildings (along the streets) and an inner courtyard with vegetation. This yard has a lower radiometry and appears as a dark linear feature in the SAR image, inducing false alarms in the road detection process.

As for the two orthogonal views, the road extraction is improved, but in a different way. Here, we have a means to classify the network depending on the confidence we have in the detection.

If we try to quantify the improvement, the following results can be found (for the whole image):

- the cross-validation of a road section by the two images would reduce the false alarm rate by about 10% in this part of the image (a road section is classified as a false alarm if it does not correspond to the network, even if its size is small⁵);
- in return, the number of non detected roads will increase, but only by 1 %.

IV. CONCLUSION AND FURTHER WORK

This article has presented a road detection method which is an adaptation of previous work to the case of dense urban area. The clique potentials have been modified to take into account more adapted knowledge. In a second part, the use of two different views for road detection purposes has been studied. It has been shown that whatever the configurations (perpendicular-complementary information-, or anti-parallel-redundant-), the road detection is improved. In the first case, the network can be completed, since some of the roads are only visible in one view. In the second case, the detection quality is improved, since the parts of the network which are not reliable can be pointed out.

One of the remaining problems is that the user has to choose the model to use. Particularly, the model proposed in this article favors 90° cross-roads which will not be adapted for historic

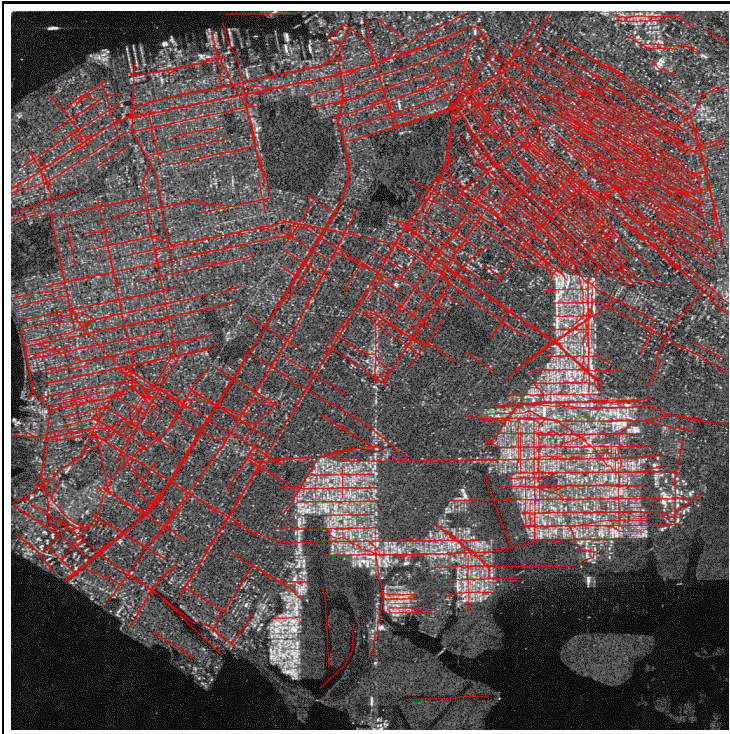
European towns for instance. A possible solution, subject of further work, is to have many models corresponding to different labels (one for river, one for roads in urban areas, one for “countryside” roads,...) and make them compete in the same optimization process.

Other works include the use of the extracted network for different applications. One of them is the use of the roads for urban characterization and classification (delimitation of interest areas, city planning indicators,...). In the same way, it could be used for data mining for which the network attributes could be a characterization of the towns. Other applications are the automatic registering of images using the extracted networks (the main difficulty being the displacement of the roads due to the lay-over effects), and the automatic determination of the ground elevation with stereo or interferometric data [18].

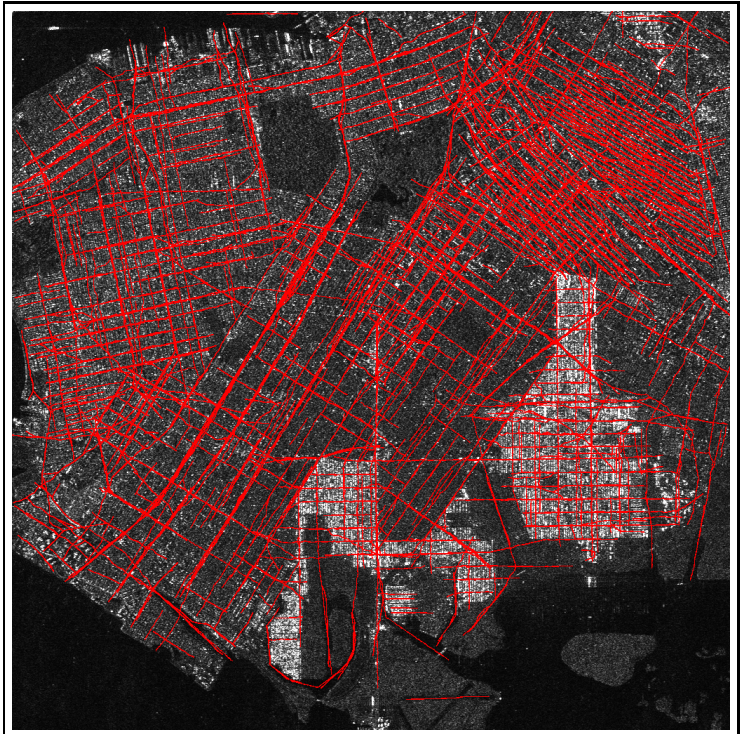
REFERENCES

- [1] R. Jordan. Shuttle radar topography mission system functional requirements document. Technical report, JPL D-14293, 1997.
- [2] web site of DLR : <http://www.dfd.dlr.de/>.
- [3] P. Gamba, B. Houshmand, and M. Saccani. Detection and extraction of buildings from interferometric SAR data. *IEEE Transactions on Geoscience and Remote Sensing*, 38(1):611–618, 2000.
- [4] D. Geman and B. Jedynak. An active testing model for tracking roads in satellite images. *IEEE Transactions on Pattern Analysis and Machine Intelligence*, PAMI-18(1):1–14, 1996.
- [5] A. Hendry, S. Quegan, and J. Wood. The visibility of linear features in SAR images. *IGARSS’88 (Edinburgh, Scotland)*, pages 1517–1520, 1988.
- [6] B. Houshmand P. Gamba. Three-dimensional road network by fusion of polarimetric and interferometric SAR data. *IGARSS’99*, 1:302–304, 1999.
- [7] F. Tupin, H. Maître, J-F. Mangin, J-M. Nicolas, and E. Pechersky. Detection of linear features in SAR images: application to road network extraction. *IEEE Transactions on Geoscience and Remote Sensing*, 36(2):434–453, March 1998.
- [8] F. T. Ulaby, F. Kouyate, B. Brisco, and T.H. L. Williams. Textural information in SAR images. *IEEE Transactions on Geoscience and Remote Sensing*, 24(2):235–245, March 1986.
- [9] R. Touzi, A. Lopes, and P. Bousquet. A statistical and geometrical edge detector for SAR images. *IEEE Transactions on Geoscience and Remote Sensing*, 26(6):764 – 773, November 1988.
- [10] J.W. Goodman. Some fundamental properties of speckle. *Journal Optical Society of America*, 66(11):1145–1150, 1976.
- [11] C. Gouinaud, F. Tupin, and H. Maître. Potential and use of radar images for characterization and detection of urban areas. *IGARSS’96 (Nebraska)*, 1:474–476, May 1996.
- [12] C. Oliver and S. Quegan. *Understanding Synthetic Aperture Radar Images*. Artech House publishers, 1998.
- [13] E. S. Deutsch. Thinning algorithms on rectangular, hexagonal, and triangular arrays. *CACM*, 15(9):827–837, 1972.
- [14] R. D. Duda and P. E. Hart. Use of the hough transformation to detect lines and curves in pictures. *Comm. ACM*, 15(1):11–15, 1972.
- [15] E. Prisner. Line graphs and generalizations, a survey. *Congressus Numerantium*, 116:193–229, 1996.
- [16] D. Riviere, J-F Mangin, J-M Martinez, F. Chavand, and V. Froin. Neural network based learning of local compatibilities for segment grouping. *SSPR’98, LNCS 1451, Sydney*, pages 349–358, 1998.
- [17] F. Tupin. Radar cross-views for road detection in dense urban areas. *EU-SAR 2000, Munich*, pages 617–620, 2000.
- [18] F. Tupin and M. Roux. Markov random fields for Digital Terrain Model extraction. *IEEE/ISPRS Joint Workshop on Remote Sensing and Data Fusion over Urban Areas (Rome)*, pages 95–99, 2001.

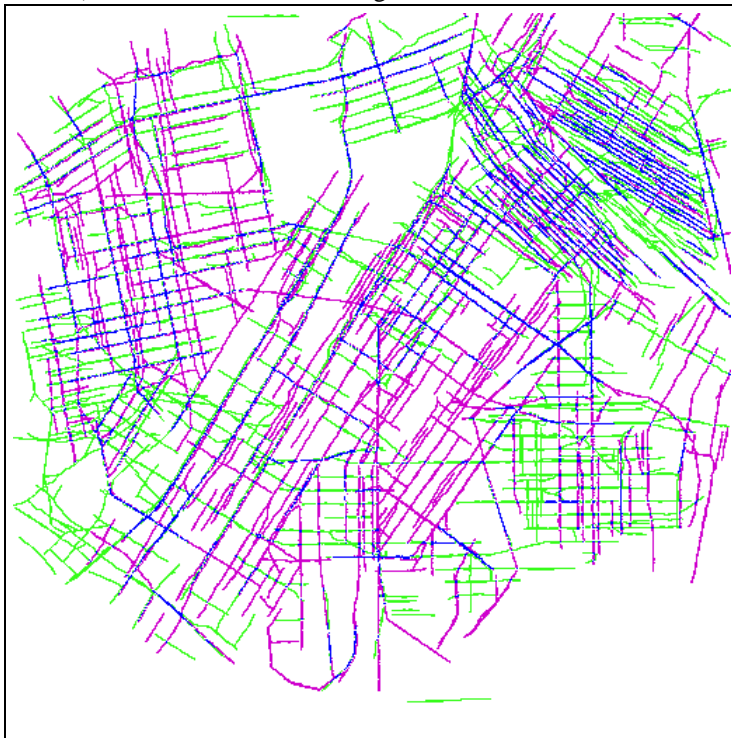
⁵which means that the global false alarm rate is over-estimated.



a) Automatic extraction using 1 view



b) Automatic extraction using 2 views



c) the 3 networks -see caption-



d) corresponding map

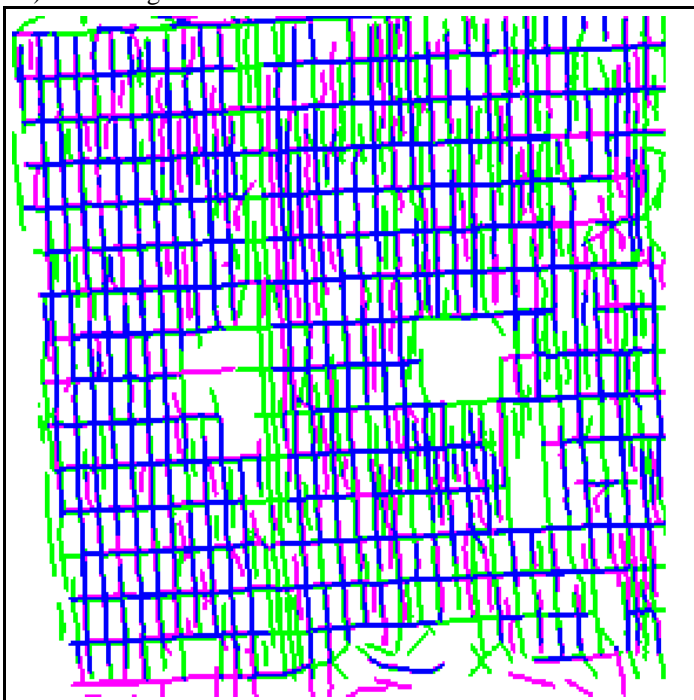
Fig. 6. Result of the road extraction process for the New-York image: top left using one view, top right using two orthogonal views (the networks extracted on each view are superimposed); on the bottom, the three networks: in blue the network detected on both views, in green the one detected on the south view only, in pink the one detected on the east view only; bottom right, the corresponding map.



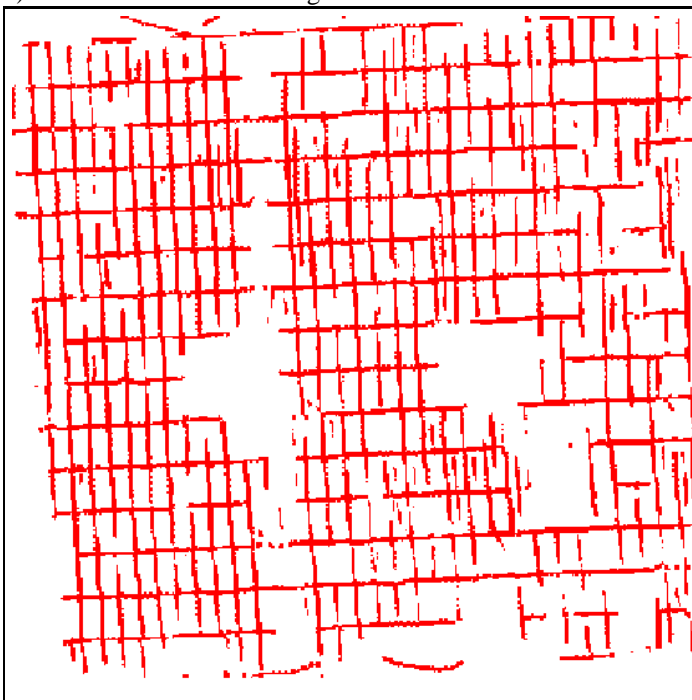
a) SAR image



b) Automatic extraction using 2 views



c) the 3 networks -see caption-



d) network detected on both views

Fig. 7. Part of the SAR view of San Francisco (pixel-spacing 5m) and the automatic extraction. The color legend for figure c) is: in blue the network detected on both views, in green the one detected on the south view only, in pink the one detected on the north view only.



Fig. 8. Image of San Francisco (size is 4000×1500 pixels) on the top and result of the road extraction process on the bottom.



Florence Tupin She received the engineering degree from Ecole Nationale Supérieure des Télécommunications (ENST) of Paris in 1994, and the Ph.D. degree from ENST in 1997. She is currently Associate Professor at ENST in the TSI (Image and Signal Processing) Department. Her main research interests are image analysis and interpretation, Markov random field techniques, and SAR remote sensing.

Bijan Houshmand Bijan Houshmand is with the Radar Science and Engineering, Jet Propulsion Laboratory, Pasadena, California, and an adjunct Associate Professor in the Electrical Engineering Department at the University of California at Los Angeles. His research activities include electromagnetic modeling for scattering and remote sensing applications, sensor fusion, image classification, and microwave system analysis and design.



Mihai Datcu Mihai Datcu received the M.S. and Ph.D. degrees in Electronics and Telecommunications from the University "Politehnica" of Bucharest UPB, Romania, in 1978 and 1986. In 1999 he received the title "Habilitation à diriger des recherches" from Université Louis Pasteur, Strasbourg, France. He holds a professorship in electronics and telecommunications with UPB since 1981. Currently he is Senior Scientist and Image Analysis research group leader with the Remote Sensing Technology Institute IMF, of the DLR Oberpfaffenhofen. His interest is in Bayesian inference, information and complexity theory, stochastic processes, model-based scene understanding, image information mining, for applications in information retrieval and understanding of high resolution SAR and optical observations.